Available online at www.sciencedirect.com

SCIENCE DIRECT®

Earth and Planetary Science Letters 235 (2005) 211–228

EPSL

www.elsevier.com/locate/epsl

Tectonic and climatic controls on silicate weathering

A. Joshua West*, Albert Galy, Mike Bickle

Department of Earth Sciences, University of Cambridge Downing Street, Cambridge CB2 3EQ, United Kingdom

Received 27 October 2004; received in revised form 26 February 2005; accepted 18 March 2005
Available online 31 May 2005
Editor: K. Farley

Abstract

Understanding the controls on chemical weathering, especially of silicate minerals, remains a major challenge, despite its importance in controlling the evolution of the Earth's surface. In particular, it has proved hard to distinguish the temperature sensitivity of silicate weathering rates from other factors. Here we present a new compilation of chemical and physical erosion rates in small catchments and show that silicate weathering rates are not governed by any single parameter but require consideration in multiple dimensions. The overall variation in silicate weathering rates with physical erosion rates, rainfall, and temperature can be quantitatively described by a parameterization based on considering their limiting relationships. At lower erosion rates mineral supply limits weathering. At higher erosion rates there is abundant material but kinetic and therefore climatic factors limit weathering. A predictive model describing the field data based on transport and weathering (kinetically) limited scenarios yields theoretically sensible values for fitted parameters. In the transport-limited case, the supply of silicate cations from weathering is directly proportional to the supply of material by erosion, consistent with complete leaching of cations from fresh regolith. In the kinetically limited case, weathering scales directly with runoff, as the square root of erosion rate, and with an activation energy of 74 ± 29 kJ/mol, consistent with expected values in the Earth's surface settings.

Keywords: weathering; erosion; CO_2; climate change; feedback; transport-limited

1. Introduction

Chemical weathering controls the evolution of the Earth's surface, shaping landscapes, determining nutrient supply to ecosystems, and regulating global chemical cycles. Silicate weathering in particular is thought to control global climate over long time scales through the consumption of atmospheric CO_2 that is eventually stored as carbonates in the oceans. This process is governed by the rate of carbonic acid dissolution reactions, as originally proposed by Ebelmen [1]:

$$2CO_2 + 3H_2O + CaAl_2Si_2O_8 = Ca^{+2} + 2HCO_3^- + Al_2Si_2O_5(OH)_4 \quad (1)$$

which should theoretically depend on mineral type reactivity, the supply of minerals, water and acid

* Corresponding author.
E-mail address: joshwest@cantab.net (A.J. West).

0012-821X/$ - see front matter © 2005 Elsevier B.V. All rights reserved.
doi:10.1016/j.epsl.2005.03.020

reactants, and an Arrhenius rate law [2]. The temperature-dependence of this reaction in Earth surface settings is thought to provide the feedback that regulates climate over geological time [3,4] and maintains equable climatic conditions on Earth [5]. This lends particular importance to distinguishing the role of temperature from other factors influencing the carbonic acid dissolution reaction.

Lithology is thought to exert a major control on weathering rate [6] by influencing the availability of minerals with varying reactivity. Silicate rocks can be divided very broadly between the more reactive mafic lithologies (such as basalts) and the less reactive felsic lithologies (such as granites and meta-pelites) for modelling weathering at the global scale [7]. Mafic rocks have minerals with a greater proportion of the Ca and Mg to supply for carbonate formation, but these are also present in felsic rocks.

Acidity drives the dissolution reaction and is predominantly supplied from atmospheric CO_2, either in soil waters or as organic acids produced by vegetation. The independent effects of vegetation have been assessed thoroughly elsewhere and for modern environments at the global scale can be assumed to be in close relationship with temperature and runoff [8,9].

The other controls on the weathering reaction are the supply of water and mineral reactants. This means that, for a given rock type at contemporary pCO_2, weathering should depend principally on temperature, runoff, and erosion rate. It has proved particularly hard to separate the roles of these factors (e.g., [10,11]), in particular whether climate or erosion govern global weathering fluxes. Even the premise that weathering rates depend on temperature has been contested [12].

A major problem has been that previous interpretations of weathering in field settings have produced conflicting results. Many studies have focused on quantifying the importance of temperature and runoff, first in granitic environments (e.g., [11] among others), and more recently for basalts (e.g., [13]). Though insightful, climatic descriptions alone provide inadequate descriptions for some environments. In cases that do not fit to simple climate-dependent trends, weathering has typically been described in broad qualitative terms as being influenced by soil cover and depth (e.g., [14]) without more detailed consideration. Other recent studies have meanwhile emphasized the apparent importance of mechanical erosion for weathering rates, whether in uniform catchments [15,16], in soil profiles [17,18], or in large heterogeneous river basins [19]. At the scale of the world's largest rivers, mechanical processes are clearly important, but they do not uniquely explain the scatter in the data. In addition, purely physical explanations do not account for the clear climatic dependence of weathering in many restricted settings.

Apparently contradictory results from these and numerous other similar studies have meant that development of a unified, quantitative description of global weathering rates has proved challenging. However, the substantial recent work on the subject offers the opportunity for a new synthesis. In the present study we have assembled a new global compilation of data on weathering rates. We show that the influence of erosion rate, temperature, and runoff on chemical weathering rates can be distinguished and quantified. The parameterization of silicate chemical weathering rates is achieved by considering the physical basis that controls chemical dissolution in Earth surface settings.

2. Methods of data compilation and analysis

2.1. Data source

This section gives an overview of the approach used in assembling the data for this study. Details of the data sources are provided in Table 1. The data compilation (Table 2) is based on chemical weathering fluxes determined from surface water chemistry and discharge, adjusted by variable means for atmospheric deposition and for the contribution from carbonates, as discussed below. The data is restricted to weathering fluxes determined by solute export in surface waters, rather than by rates determined from chemical depletion profiles in weathered regolith (e.g., [18]), which differ in both temporal and spatial scale. Temperature and runoff are reported average annual values, from the cited studies or else from regional governmental monitoring data, where noted in Table 2.

2.2. Setting

Data in the compilation are from two settings: stable continental cratons and small catchments under-

lain by granitic and meta-pelitic rocks. The stable continental cratons are the West African Shield (tributaries of the Congo, Niger, and Nyong), the Siberian Craton (tributaries of the Lena), the Guyana Shield (some tributaries of the Orinoco), and the Canadian Shield (tributaries in the Slave and Grenville Provinces). Their large basin size means that many of these tributaries integrate multiple lithology types; for example tributaries of the Lena drain metamorphosed mafic rocks as well as crystalline basement. However this heterogeneity is unimportant because of the homogeneity of the weathering environments, so that the range in weathering fluxes is small at the scale of comparison in the data set.

In more rapidly eroding settings, large basins integrate highly variable environments. The second data category therefore comprises smaller catchments (surface area $<10^3$ km^2) where these variations are small and weathering conditions can be well constrained. These catchments are restricted to those draining only granite and felsic meta-pelite lithologies, in order to limit variations introduced by lithology. To explore the impact of landscape characteristics, the small catchments were divided into sub-montane environments (defined as soil mantled, vegetated catchments) and alpine and glaciated environments (defined as catchments dominated by bare bedrock and glacial ice).

2.3. Calculation of weathering fluxes

Four weathering fluxes are reported in Table 2, all in tons/km^2/yr: total cation denudation rate (TCDR), silicate cation denudation rate (SCDR), the SiO_2 weathering rate (SiO_2 WR), and the total chemical weathering rate (CWR). The total cation denudation rate is the total flux of crustally-derived Ca+Mg+Na+K, while the silicate cation denudation rate is specifically the silicate-derived Ca+Mg+Na+K, the flux which moderates atmospheric CO_2 contents. These are reported in elemental weight units because of their importance for global element cycles. The CWR is the total mass of material lost by chemical weathering, calculated as:

$$\mathrm{CWR} = \mathrm{CaO_{weath}} + \mathrm{MgO_{weath}} + \mathrm{Na_2O_{weath}} + \mathrm{K_2O_{weath}} + \mathrm{SiO_{2weath}} + \mathrm{CO_{2carbweathering}}$$

where $CO_{2carbweathering}$ reflects the carbon lost in the weathering of carbonate, calculated based on a molar 1:1 ratio with the $(Ca+Mg)_{carbweathering}$ measured in solute loss. Flux values reported in the literature were used as published (see details in Table 1). Where not published, they were calculated as the product of appropriately adjusted chemical concentration, either from spot sampling or annual averages, and annual discharge.

Where correction was not made for atmospheric deposition in the literature, silicate-derived Na* was calculated by adjusting based on a precipitation Na/Cl ratio of 0.87, reflecting sea salt composition. Universally low ratios of other cations and silica to Cl in deposition mean only very minor (<5%) undercorrection of these fluxes. Silicate derived Ca_{sil} and Mg_{sil} were then determined based on common molar ratios of Ca_{sil}/Na^* (0.35) and Mg_{sil}/Na^* (0.24) from silicate weathering, estimated from global stream chemistry [19]. These ratios are applied universally for all catchments because the compilation is restricted to felsic lithologies, except for the continental cratons where the range in weathering rates is very small. All dissolved K was assumed to derive from silicates. This does not correct for evaporite contribution to dissolved load, but there are no known salt deposits in any of the small basins compiled here, and low Cl/Na ratios mean an undercorrection that is within the error of the data.

This calculation procedure ignores both the heterogeneity of silicate sources and the temporal variability of concentration–discharge relationships, with estimated 2σ uncertainty of 30% and 25%, respectively [20], small enough to allow meaningful comparison at the scale of comparison in our data set. The errors quoted in Table 2 include this error plus an uncertainty based on the observed variability of multiply sampled catchments from each region. In cases where silicate weathering fluxes were calculated separately in the literature, the procedure used here agrees within 20% of published values.

The average values reported in Table 2 reflect more than nineteen data points, because in all but four cases, each value is a regional average for more than one catchment or tributary. For regions with a small number of tributaries, but where some tributaries were sampled in multiple years, each yearly value was considered separately in the calculation of regional averages.

Table 1
Description of data sources for each region

	Chemistry data type	Deposition correction	Silicate Ca and Mg components	Erosion rates	Specific notes
Canadian Shield	Annual discharge and spot chemistry samples	Ratio correction to Cl by Millot et al. [15]	Standard Ca/Na and Mg/Na ratios	Average regional rates from suspended sediment fluxes estimated by Millot et al. [15]	5 rivers of Slave Province (Yellowknife sampled twice); 6 rivers of Grenville Province (Mistassinni sampled 3 times)
Siberian Shield	Annual discharge and spot chemistry samples	Seasalt Na/Cl ratio	Standard Ca/Na and Mg/Na ratios	Suspended sediment flux of Lena River, draining entire region	All rivers draining Anabar Shield, Trans-Baikal Highlands, and Aldan Shield
African Shield	Annual discharge and spot chemistry sample	Congo and Nyong: seasalt Na/Cl ratio; Niger: ratio correction to Cl by Picouet et al. [40]	Standard Ca/Na and Mg/Na ratios	Spot sampling of suspended sediment and annual discharge for four tributaries of the Congo and two of the Niger	Tributaries of the Congo, Niger, and Nyong (Likouala and Soumou not included because of suspicious Cl data)
Guyana	Annual discharge and spot chemistry samples	Ratio correction to Cl by Edmond et al. [41]	Standard Ca/Na and Mg/Na ratios	Reported discharge and spot sampling of suspended sediment for all nine basins	Nine basins of shield area (2 have calculated SCDR>TCDR but within 1σ error)
Appalachians	Variably determined element budgets compiled by White et al. [11]	Measured precipitation input fluxes for each element; Si inputs assumed zero where not reported (maximum 4% of outputs where available)	Standard Ca/Na and Mg/Na ratios	Cosmogenics in sediments from Great Smoky Mountains; spatially uniform and assumed to represent entire region; also agree with estimates from sediment fluxes elsewhere in region	Nine Appalachian region catchments from White et al. [11] with non-negative weathering budgets for all major elements (including negative Na budgets for Indian River and negative K budgets for Cadwell Creek, Mundberry Brook, Panola, and Woods Lake would decrease estimated SCDR by 12%, within our error)
Idaho	Annual averaged element budgets	Corrected by Clayton and Megahan [42] based on measured input fluxes	Standard Ca/Na and Mg/Na ratios	Cosmogenics in sediments of six basins (SC2, SC3, SC5, SC6, SC7, and SC8); order of magnitude higher than sediment flux measurements which missed large high magnitude events [22]	Chemical data reported as average for four Silver Creek basins over multi-year study (SC1, SC2, SC5, and SC6)

British Columbia	Annual averaged element budgets	Measured precipitation input fluxes for each element	Standard Ca/Na and Mg/Na ratios	Sediment accumulation rate in downstream basin	Data from monitoring of 1 catchment
Sabah Malaysia	Annual averaged element budgets	Measured precipitation input fluxes for each element	Standard Ca/Na and Mg/Na ratios	Annual average stream sediment flux	Data from monitoring of 2 catchments
Cote d'Ivoire	Annual average element budgets	Measured inputs calculated as annual average rain chemistry times rainfall total plus reported dust chemistry times dust deposition rate	Standard Ca/Na and Mg/Na ratios	Annual average stream sediment flux	Stream outputs calculated by separating average baseflow and average quickflow chemistry and calculating for annual baseflow and quickflow rates
East NZ Alps	Annual discharge and spot chemistry samples	Seasalt Na/Cl ratio	Standard Ca/Na and Mg/Na ratios	Reported discharge and spot sampling of suspended sediment for all seven basins	Seven basins east of Divide, 3 sampled twice
Lesser Himalaya	Annual average element budgets	Corrected by West et al. [16] based on measured precipitation input fluxes for each element	Mineral mass balance [16]	Cosmogenics in sediment of Alaknanda River in India for equivalent Himalayan setting; 2σ overlaps with range of locally measured sediment fluxes	Two small catchments in central Nepal
Puerto Rico	Annual average element budgets	Ratio correction to Cl by Turner et al. [38]	All chemical flux assumed to be silicate [38]	1. Long term estimate from chemical mass balance and cosmogenics 2. Modern day estimate from suspended sediment flux	Well studied basin; use data from most recent work on solute budgets (not regolith depletion which measures different process)
Colorado Rockies	Annual average element budgets (average over 1993 and 1994)	Measured precipitation input fluxes for each element	Standard Ca/Na and Mg/Na ratios	Cosmogenics in sediments from catchments elsewhere in Colorado Front Range	Chemistry from nine basins, with glacial cover; cosmogenics from other non-glaciated basins elsewhere in mountain range
Sierra Nevada, U.S.	Variably determined element budgets compiled by White et al. [11]	Measured precipitation input fluxes for each element	Standard Ca/Na and Mg/Na ratios	Cosmogenics in sediments from catchments elsewhere in Sierra Nevada	Chemistry from three Sierra Nevada catchments from White et al. [11], partial glacial cover; cosmogenics from other non-glaciated basins elsewhere in mountain range

(continued on next page)

Table 1 (*continued*)

	Chemistry data type	Deposition correction	Silicate Ca and Mg components	Erosion rates	Specific notes
Svalbard	Annual average element budgets	Corrected by Hodson et al. [43] based on measured precipitation input fluxes for each element	Standard Ca/Na and Mg/Na ratios	Average sediment flux from four Svalbard basins, three (Broggerbreen, Hannabreen, and Erikbreen) matching basins where chemical fluxes measured	Chemistry from six basins, three measured over two-year periods
Swiss Alps	Annual average element budgets	Corrected by local precipitation ratios to Cl by Hosein et al. [44]	Annual average element budgets	Annual average local stream sediment flux	Two basins, one monitored over 2 yr, both partially glaciated, one with massive carbonate outcrop
High Himalaya	Annual average element budgets	All three catchments corrected by measured inputs	Two catchments by mineral mass balance [16]; one by standard ratios [45]	Cosmogenics in sediment of Alaknanda River in India for equivalent Himalayan setting; 2σ overlaps with estimate from chemical mass balance of Ganges basin [46]	Three partly glaciated basins: Langtang Lirung in central Nepal and Dokriani in Garwhal [16]; Batura in Nanga Parbat [45]
West NZ Alps	Annual discharge and spot chemistry samples	Seasalt Na/Cl ratio	Standard Ca/Na and Mg/Na ratios	Reported discharge and spot sampling of suspended sediment for all six basins	Six basins west of the Divide

Table 2
Weathering rate data compilation

	SCDR ($t/km^2/yr$)	TCDR ($t/km^2/yr$)	SiO_2 WR ($t/km^2/yr$)	CWR ($t/km^2/yr$)	TDR ($t/km^2/yr$)	R (mm/yr)	T (°C)	Lithology	n
Shields/cratons (homogeneous weathering environment)									
Slave, Canada	0.25 ± 0.05 [15]	0.66 ± 0.14	0.18 ± 0.17	1.17 ± 0.29	3.2 ± 0.9 [15]	100	−4.0	G	6, 1[a]
Siberia	0.77 ± 0.27 [12]	4.18 ± 1.10	1.61 ± 0.40	10.00 ± 2.60	15 ± 8.3 [24]	270	2.0	G/H/L	21, 1[a]
Africa	0.80 ± 0.25 [47,48,40]	1.31 ± 0.36	2.96 ± 0.63	5.33 ± 1.17	10 ± 2.3 [47,48]	250	24.1	G	29, 6
Grenville, Canada	1.14 ± 0.23 [15]	2.21 ± 0.45	2.63 ± 0.53	5.56 ± 1.21	13 ± 3.4 [15]	580	4.5	G	9, 1[a]
Guyana	2.40 ± 0.64 [41]	2.52 ± 0.65	10.18 ± 2.46	13.71 ± 3.35	35 ± 7.5 [41]	1680	25.0	G/H/L	9, 9
Sub-Montane Catchments (soil mantled, mixed vegetation, some agriculture)									
Appalachians	1.26 ± 0.27 [11]	2.02 ± 0.50	4.77 ± 1.09	8.19 ± 1.81	73 ± 15 [23]	850	8.9	G/H/L	9, 25[a]
Idaho Batholith	2.46 ± 0.53 [42]	2.90 ± 0.65	7.74 ± 1.94	12.10 ± 2.72	177 ± 44 [22]	390	4.5[b]	G	6, 4
British Columbia	2.49 ± 0.62 [49]	5.52 ± 1.37	9.13 ± 2.34	20.49 ± 5.00	43 ± 11 [49]	3670	9.9[b]	G	1, 1
Sabah Malaysia	3.35 ± 1.16 [50]	4.05 ± 1.39	5.86 ± 1.99	12.79 ± 4.34	48 ± 12 [50]	1960	25.7[b]	L	2, 2
Cote d'Ivoire	4.54 ± 1.14 [51]	4.37 ± 1.08	11.83 ± 3.04	17.91 ± 4.37	168 ± 51 [51]	470	26.0	G	1, 1
East Southern Alps	5.09 ± 1.15 [29]	16.88 ± 4.06	9.87 ± 2.13	46.80 ± 11.06	989 ± 210 [29]	1690	13.0	H	10, 10
Lesser Himalaya	9.69 ± 1.99 [16]	13.25 ± 2.65	N.A.	N.A.	2080 ± 460 [16,52]	1290	14.5	L	2, 4[a]
Puerto Rico Long Term	15.97 ± 3.99 [38]	15.97 ± 3.95	24.25 ± 6.23	46.67 ± 11.4	159 ± 40 [38]	3680	22.0	G	1, 1
Puerto Rico Modern Day	15.97 ± 3.99 [38]	15.97 ± 3.95	24.25 ± 6.23	46.67 ± 11.4	1000 ± 320 [38]	3680	22.0	G	1, 1
Alpine Catchments (bare bedrock, partial glacial cover)									
Colorado Rockies	0.65 ± 0.15 [53]	1.17 ± 0.26	1.76 ± 0.4	4.00 ± 0.88	343 ± 72 [54]	580	5.8[b]	G/H	7, 13[a]
Sierra Nevada	0.91 ± 0.32 [11]	1.17 ± 0.41	2.57 ± 0.52	5.49 ± 1.43	167 ± 37 [17]	1410	6.0	G	3, 22[a]
Svalbard	0.99 ± 0.32 [43]	6.97 ± 1.53	0.45 ± 0.12	18.29 ± 4.02	1019 ± 302 [55]	980	−4.6	G/H	9, 4
Swiss Alps	2.39 ± 0.52 [44]	7.13 ± 2.49	9.91 ± 2.01	34.68 ± 12.8	585 ± 139 [44]	2840	0.5	G/H	3, 3
High Himalaya	5.78 ± 1.38 [16]	22.76 ± 5.49	3.35 ± 0.72	50.38 ± 11.5	7020 ± 1430 [52]	2060	5.0	H	3, 2[a]
West Southern Alps	25.79 ± 6.01 [29]	98.54 ± 23.4	31.19 ± 6.56	249.02 ± 58.0	11549 ± 2580 [29]	7380	10.0	H	6, 6

SCDR = silicate cation denudation rate (see text); TCDR = total cation denudation rate; SiO_2 WR = SiO_2 weathering flux; CWR = total chemical mass flux from weathering; TDR = total physical + chemical denudation rate; R = average annual runoff; T = average annual temperature. Lithology: G = granite/diorite, H = high grade metapelites, L = low grade metapelites/sandstones; n = number of catchments per region, first number refers to number for chemical and second for physical erosion values.

[a] Average regional physical erosion rate, not specific to individual tributaries used for chemical flux calculation.

[b] Temperature from regional monitoring.

2.4. Calculation of physical erosion fluxes

Total denudation rates are based on either sediment flux data or erosion rate estimates from cosmogenic nuclide accumulation in sediments, as detailed in Table 1. Where literature values are reported as physical erosion rates (for all sediment-based measurements and some cosmogenic), total denudation rates reported in Table 2 were calculated as the sum of physical erosion rate plus the calculated total chemical weathering rate. The coupling of cosmogenic and sediment derived data is imperfect but justifiable for the purpose of our analysis. Cosmogenic isotope analysis of river sediment measures long term average erosion rates (e.g., [21] among others) and is used because in some rapidly eroding settings dominated by infrequent high-magnitude events, short-term sediment yield may substantially underestimate denudation rates [22]. In contrast, in more slowly eroding terrains, erosion rates are broadly uniform over short and long time scales in the absence of major land use changes [23]. The data compilation therefore relies on cosmogenic estimates where these are available, particularly in the rapidly eroding catchments, supplemented in other cases by sediment flux data.

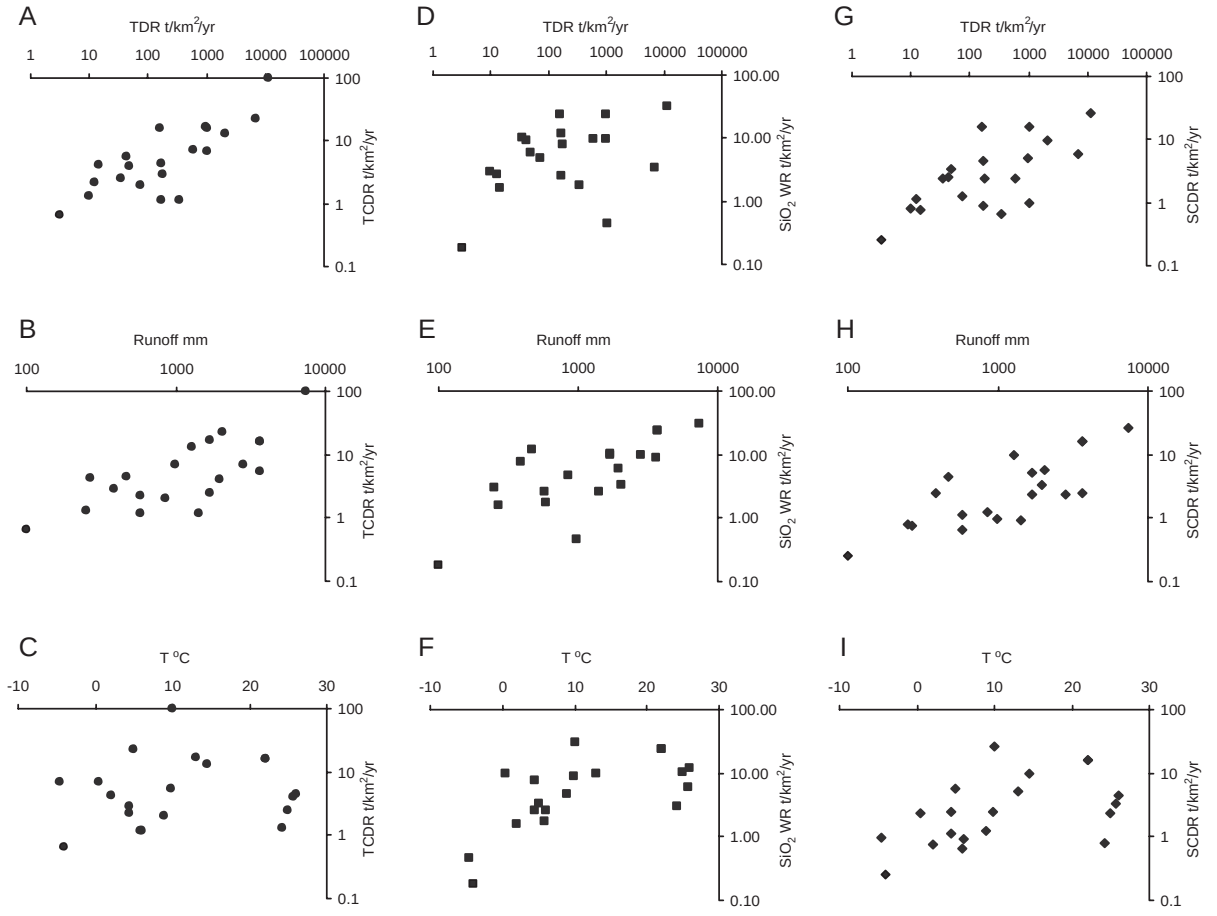

Fig. 1. Relationships between three measures of weathering rate (TCDR = total cation denudation rate; SCDR = silicate cation denudation rate; SiO_2 WR = SiO_2 weathering rate) and total denudation rate (TDR) (a), runoff (b), and temperature (c) for our dataset. Total cation weathering rate shows good relationship with total denudation and runoff, reflecting control by material supply. Silicate weathering, reflected by both total silicate cation and SiO_2 weathering rates, is more sensitive to temperature, except at very high temperatures where weathering rates are low. Models understanding silicate weathering must take into account both the major trends and their deviations.

Directly coupled physical and chemical data were available for most but not all catchments. Elsewhere data represent separate averages of erosion rate and weathering rate for catchments from the same region (see details in Table 1). In two cases (Sierra Nevada and Colorado Front Range) they combine erosion rate data from non-glacial and weathering rate data from some partly-glaciated catchments. This offers a poor basis for comparison but these points make an insignificant difference to the analysis and do not differ from partly glaciated catchments (e.g., Swiss Alps, Svalbard) where physical and chemical fluxes are derived from the same basins. Their good fit to the model (see Discussion) despite possible expected differences suggests that in these cases total denudation rates may not differ at the scale of our analysis between unglaciated catchments and nearby terrains with very small glaciers such as those found in Colorado and the Sierra Nevada.

3. Results

Total cation, silicate cation, and SiO_2 weathering rates are shown in Fig. 1 in relation to physical erosion rate, runoff and temperature. Physical erosion and runoff both relate most directly to the total cation weathering rate (Fig. 1A,B), pointing to the important role of reactant supply in controlling overall chemical denudation. However, there is substantially more scatter in their relationship with measures of silicate weathering, the SiO_2 (Fig. 1D,E) and silicate cation (Fig. 1D,E) weathering rates. Conversely, total cation weathering rate shows little correlation with temperature (Fig. 1C) whereas the measures of silicate weathering exhibit distinct relationships with temperature (Fig. 1F,I). The influence of runoff and mechanical erosion, rather than temperature, on total chemical denudation rates is consistent with previous conclusions for the world's largest river basins [19,24]. It suggests that, at least for total weathering rates, processes at the scale of the homogeneous catchments in this study are similar to those at the scale of large heterogeneous basins.

In terms of silicate weathering specifically, the field data demonstrate no single control on weathering rates even though there are broadly positive relationships for all three factors. The most obvious discrepancy is that warmer environments generally mean higher chemical weathering rates, but some extremely hot environments paradoxically appear to have extremely low silicate cation weathering rates. Similarly, despite a general positive correlation with physical erosion rate, silicate cation weathering rates in some cases show no change, or even decrease, despite a three order of magnitude increase in erosion rate. It is these and similar paradoxes that have challenged the understanding of silicate cation weathering rates at the watershed scale and hampered a general predictive explanation of the factors regulating silicate weathering rates globally. Weathering rate could be considered a simple function of erosion, and the scatter ignored as inherent uncertainty, but this would not account for the positive relationship with temperature in many cases. Consideration of the rate-limiting processes at both low and high erosion rates (cf. transport and weathering limited regimes [25,26]) provides the basis for a more complete analysis of weathering dependencies.

4. Discussion

4.1. Limits on silicate weathering rates: transport limitation

When the supply of water and acid relative to the supply of silicate minerals is large, and the residence time in the weathering environment compared to reaction time is long, minerals are nearly completely altered before their removal. Nearly complete leaching of cations would mean that silicate cation weathering rates (ϖ)–variables and units defined in Table 3–should be directly related to total erosion rate (ε) by

$$\varpi = A \cdot \varepsilon \quad (2)$$

where the constant, A, is the weight fraction of soluble cations in silicate rock. The continental cratons define a linear array on the logarithmic plot of chemical weathering versus physical erosion rate (Fig. 2), with a slope close to one (0.96 ± 0.09, 1σ) and a value of $A = 0.08 \pm 0.02$, comparable to the weight fraction of Ca+Mg+Na+K (0.1) in average silicate upper crust [27], as predicted by Eq. (2). In these cases, along with the other small catchments that lie on the regression line in Fig. 2, weathering rates are controlled by physical erosion rates rather than by

Table 3
Definition of symbols used in the text

Symbol	Meaning	Units
ϖ	silicate cation denudation rate	t/km^2/yr
ε	material supplied by total denudation	t/km^2/yr
E	total denudation rate	km/yr
A	weight fraction soluble cations	t cations/t rock
W	kinetic rate of weathering	yr^{-1}
τ	residence time	yr
ϖ_k	kinetically dependent weathering rate	t/km^2/yr
ω_v	instantaneous volumetric chemical weathering rate	t/km^3/yr
t	time in weathering environment	yr
ρ	density	g/cm^3
Γ	runoff	mm/yr
T	temperature	°K
K	kinetic weathering coefficient	t/km^2/yr
C	kinetic weathering intercept	t/km^2/yr
E_a	activation energy	kJ/mol
R	gas constant	8.3144 J mol^{-1} K^{-1}
α	erosion exponent	–
β	runoff exponent	–

kinetic constraints on reaction rates. The close relationship between chemical and physical processes implied by Eq. (2) is determined by the rate of material supply and removal from landscapes ([25,26,28]). When removal processes are slow relative to chemical weathering rates, chemical weathering rates become "transport limited", that is determined by the supply of solids by erosion. A requirement for such transport-limited weathering regimes is that sufficient time must have elapsed after changes in erosion rate or climate for the chemical weathering processes to return to equilibrium with supply of material. This time scale is presumably that required for the development of thick soils prior to which weathering rates might be expected to exceed those predicted by Eq. (2).

4.2. Limits on silicate weathering rates: kinetic limitation

Silicate cation and SiO_2 weathering fluxes from catchments with erosion rates higher than in the "transport-limited" cases exhibit no clear correlation with erosion rate (Fig. 2). This is because silicate chemical weathering is incomplete and dependent on the kinetics of the reactions regulated by temperature, runoff and vegetation (cf. 'weathering limited', [25]). In this case, the silicate weathering rate (ϖ) depends on the kinetic rate of mineral dissolution (W), the supply of material by erosion (ε), and the time available for reaction (τ):

$$\varpi = W \cdot \varepsilon \cdot \tau \quad (3)$$

where the value of W depends on the environmental conditions such as temperature and runoff. In the

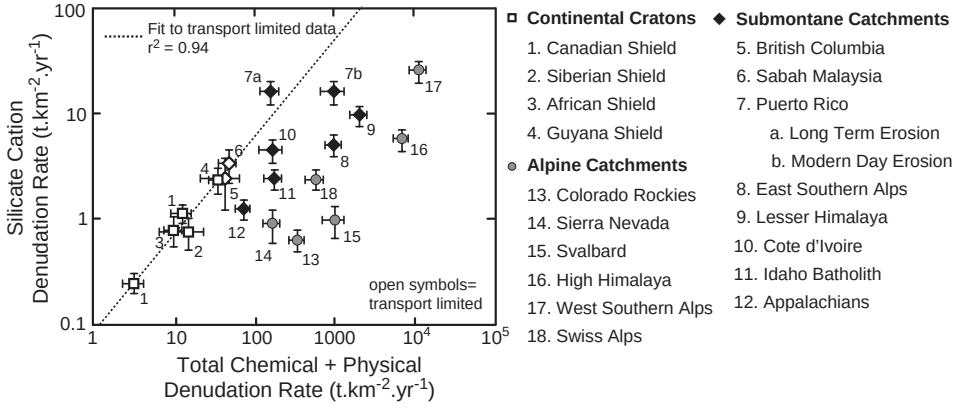

Fig. 2. Silicate cation denudation rate versus total denudation rate, illustrating the limiting conditions on silicate weathering. In transport-limited catchments (open symbols), erosion controls chemical weathering rates because material supply is limited, so weathering rates may be low despite high temperatures. Silicate cation loss varies predictably with total denudation rate as a function of complete cation leaching from regolith (see text). At higher erosion rates, silicate weathering shows substantial scatter away from this trend because, with high material supply, it becomes dependent on kinetics controlled by climatic variables such as temperature and vegetation. Error bars are 1σ errors. The regression line was fitted to transport-limited catchments by the least-squares method of York [39] which takes into account errors and correlations between errors on both x and y parameters.

simplest case, the time available for reaction is inversely proportional to the erosion rate (i.e., $\tau \propto \varepsilon^{-1}$) so that Eq. (3) simplifies to:

$$\varpi = \varpi_k \tag{4}$$

with ϖ_k being the kinetically dependent weathering rate.

In the theoretically limiting case of the highest erosion rates, silicate minerals will pass through the weathering regime rapidly and undergo infinitely limited dissolution, so that the reaction kinetics are, to first order, independent of erosion rate. As erosion rates fall below the theoretically limiting case, reaction kinetics themselves are likely to depend on erosion rate, because freshly ground mineral surfaces, which weather more rapidly, are progressively removed as material remains longer in the weathering environment. This means that ϖ_k in Eq. (4) will vary with erosion rate in realistic natural setting, consistent with the broadly positive relationship between silicate weathering fluxes and mechanical erosion rates observed in rapidly eroding basins [29].

The decrease of weathering rates with time in field settings can be described by a power law [30]. Comparison of short and long term weathering measurements [31] indicate that the instantaneous weathering rate of a given mineral or rock (ω_v) decreases with the time that the mineral spends in the weathering environment, as $\omega_v \propto t^{-\alpha}$, with $\alpha \sim 0.5$–0.7 for common minerals. For a given type of mineral, catchment weathering rates in the field represent the combination of the weathering rates of all individual mineral grains in the critical zone, some of which will have spent very little and others very long periods of time in the weathering environment. At steady state, where processes are constant over time scales longer than the residence time of the material being weathered, this is equivalent to following the history of one individual mineral grain over the course of its total time in the catchment. Integrating the instantaneous weathering rate, ω_v, of this mineral over its residence time, τ, yields the amount the mineral has weathered over its catchment history. The total weathering rate in the catchment, ϖ, is equal to this value multiplied by the rate at which the weathered material is being removed, equivalent to the erosion rate E. Thus:

$$\varpi_k \propto E \cdot \int_0^{\tau} t^{-\alpha} \mathrm{d}t \tag{5}$$

In the simplest case where the residence time is inversely proportional to erosion rate ($\tau \propto E^{-1}$), and assuming that erosion rate is proportional to the amount of material supplied by erosion ($\varepsilon = \rho \cdot E$, where ρ is the density), this equation simplifies to:

$$\varpi_k \propto \varepsilon^{\alpha} \tag{6}$$

where the kinetically dependent weathering rate from a catchment has a power law dependence on erosion rate. In many catchments, minerals pass through the weathering environment at different rates; Eq. (6) assumes that minerals have a limited range of individual residence times. Spatially heterogeneous erosion, such as that driven by landsliding, would result in more complex relationships, but determination of the most appropriate laws will require a much better understanding of the spatial and temporal controls on chemical weathering rates within catchments.

In addition to this dependence on erosion rate, the limiting kinetic control in rapidly eroding terrains might be the temperature-dependent rate at which silicate minerals react, the vegetation-dependent rate of supply of organic acids, a rainfall/runoff limited supply of water and acid or a combination of all three, with differing kinetic factors in different weathering regimes. Numerous previous efforts have used various field data to quantify these controlling kinetic parameters (e.g., [11,14,32] among others). In general, silicate chemical weathering rates have been described as lying on a surface in the three-dimensional plot against runoff and temperature [11]. A commonly assumed functionality of these surfaces [32] describes silicate weathering rate (ϖ) as a power-law function of runoff ($\varpi \propto \Gamma^{\beta}$, with exponent β often assumed to be one, e.g., [7]) and an Arrhenius rate law function of temperature ($\varpi \propto e^{-E/RT}$, with E_a the activation energy and R the gas constant). Vegetation is considered adequately described by temperature and runoff. Here we add a control on kinetics exerted by erosion

rate following from Eq. (6), so that we fit a kinetic dependence of weathering of the form

$$\varpi_k = K\left(1+\frac{\delta\varepsilon}{\varepsilon_0}\right)^{\alpha}\left(1+\frac{\delta\Gamma}{\Gamma_0}\right)^{\beta} e^{\left[-\frac{E_a}{R}(1/T-1/T_o)\right]} \quad (7)$$

where the response of weathering rate is normalized relative to the log-mean temperature (T_o=11.1 °C), the difference ($\delta\varepsilon$) from log-mean erosion rate (ε_0=412 tons/km^2/yr) and the difference ($\delta\Gamma$) from log-mean rainfall (Γ_0=1506 mm/yr) of the data set. This implies that weathering rates lie on a series of surfaces in the 3D runoff–temperature–weathering space described in previous models [11], the exact surface dependent on erosion rate.

A non-linear least-squares fit to the data on silicate cation denudation rates for kinetically limited catchments compiled in this study gives $K=2.82\pm0.39$ tons/km^2/yr, $\alpha=0.37\pm0.09$, $\beta=0.73\pm0.20$, and $E_a=63\pm14$ kJ/mol (1σ errors—see Appendix A). However there is no a priori reason why the surface defined by the function in Eq. (7) should pass through the origin, because at very low values, weathering rates are not kinetically controlled (i.e., Eq. (2)). A fit to the more general equation $\varpi_k=C+f(\varepsilon,\Gamma,T)$, where C is a constant and $f(\varepsilon,\Gamma,T)$ the function in Eq. (7), gives $K=2.28\pm1.09$ tons/km^2/yr, $C=0.34\pm0.60$ tons/km^2/yr, $\alpha=0.42\pm0.15$, $\beta=0.80\pm0.32$ and $E_a=74\pm29$ kJ/mol. Calculated uncertainties on these variables are significantly correlated (see Table 4, and description of fitting methodology in Appendix A).

The results of the model fit with five parameters, including free constant C, are shown in Fig. 3, which projects the residuals of the fit into two dimensions and shows the deviation of the points from the best-fit plane. With a few exceptions, the deviations lie close to the plane, indicating the good explanation of weathering rates for these locations by the model. The notable exceptions that lie further from the plane are all sites where the uncertainty on the measured chemical weathering rates is much higher, including the Southern Alps and Puerto Rico. The summary of the model is illustrated in the upper left panel of Fig. 3; weathering rates lie on a series of such 3D surfaces for different runoff values. Weathering is described by the kinetic equation at most erosion rates but is transport limited at very low erosion rates. At high temperature and high runoff, this area of transport-limited weathering is more significant.

4.3. Variability of kinetic thresholds and time scale of weathering

The natural variability of temperature and runoff means that the transition from kinetic to transport limitation is inevitably variable. The scatter at higher erosion rates in Fig. 2 reflects the variability of kinetic controls on weathering expressed in Eq. (7). For a constant kinetic control by temperature and runoff, the

Table 4
Results of least-squares fits to kinetically limited data

Least-squares fit with $C=0$[a]		Correlation coefficients			
α	0.37 ± 0.09		β	E_a	γ
β	0.73 ± 0.20	α	−0.41	0.47	0.09
E_a	63 ± 14	β		−0.25	−0.05
K	2.82 ± 0.39	E_a			−0.03

Least-squares fit with C a free parameter		Correlation coefficients				
α	0.42 ± 0.15		β	E_a	γ	C
β	0.80 ± 0.32	α	0.07	0.76	−0.65	0.63
E_a	74 ± 29	β		0.34	−0.59	0.60
K	2.28 ± 1.09	E_a			−0.77	0.78
C	0.34 ± 0.60	γ				−0.92

[a] Parameters are as defined for Eq. (7) (see text); 1σ errors calculated by Levenberg–Marquardt non-linear least-squares fit based on uncertainties in Table 2, with errors multiplied by ~2 to give expected χ^2 appropriate for degrees of freedom. Low error multiplier indicates good fit given the nature of the data. Note high correlation coefficients for fit with five free parameters.

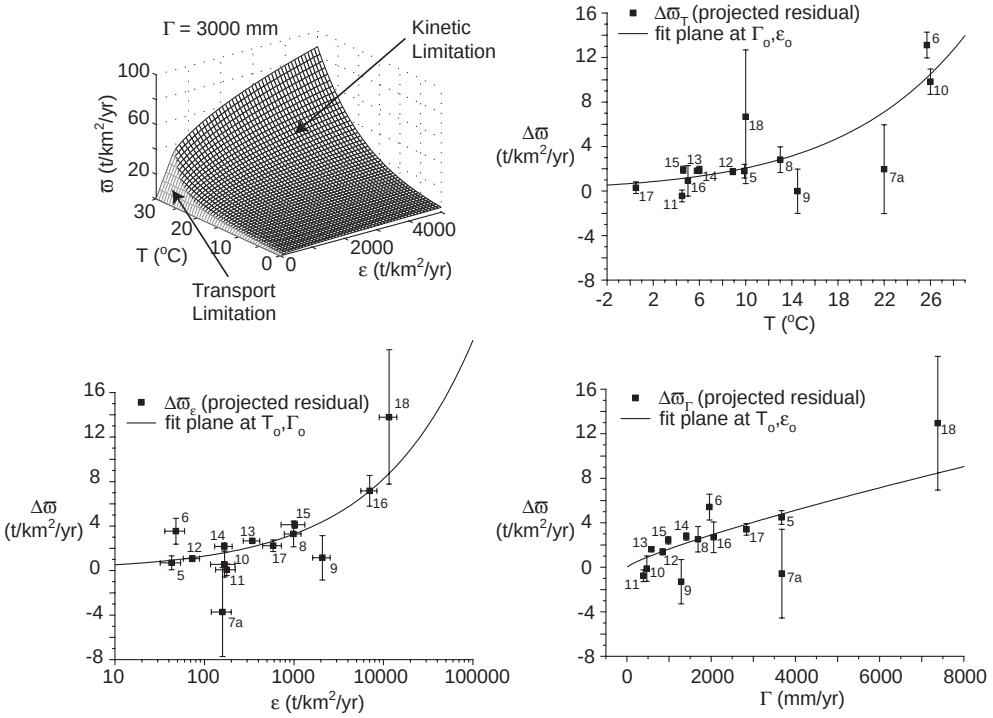

Fig. 3. Model for controls on silicate weathering, parameterized by field data. Upper left panel is a slice for a fixed runoff value (Γ = 3000 mm) through the 4D space of silicate weathering vs. erosion, temperature, and runoff; the two fields represent transport-limited (dependent only on erosion) and kinetically limited weathering regimes. The other panels show intersection of the best-fit 4D plane with the 2D section defined by average values of non-plotted variables (T_o = 11.1 °C, Γ_o = 1506 mm, and ε_o = 412 t/km^2/yr). Points ($\Delta\omega$) are the projection of the residual ($\omega_{obs} - \omega_{calc}$) into 2D and are the best representation of the data quality against each model parameter. Labels for each point correspond to the legend from Fig. 2. Error bars show 1σ errors; points without noticeable errors bars have 1σ errors smaller than the size of the point.

chemical weathering rate–erosion rate relationship on the logarithmic plot in Fig. 2 is expected to flatten from the slope of one at low erosion rates to a slope of α at high erosion rates. The range of erosion rates that characterize the transition away from the transport-limited condition must themselves be a function of the kinetic controls by temperature and runoff. This has two important implications, 1) the feedback process which moderates global climate on long time scales takes place in more rapidly eroding terrains and 2) short-term climatic fluctuations, for example from glacial–interglacial cycles, may move the transitional zone in the silicate chemical weathering to physical erosion rate relationship. Climate change will not only affect weathering rates in the most rapidly eroding terrains but also change the relative areas of crust characterized by transport versus weathering limited weathering, in addition to any dependence of erosion rate on climate. Understanding the time scale of such a change remains crucial for understanding the response of weathering systems to climatic and tectonic perturbation.

The chemical depletion of soils relative to bedrock provides one record of weathering over longer time scales. Riebe et al. [17,33,34] have coupled this depletion to spatially-averaged physical erosion rates in order to determine long-term weathering rates in actively eroding settings. By applying this method to catchments with varying climate and physical erosion rates, they have attempted a similar description of the controls on silicate weathering to that in Eq. (7) [18]. Their data do not show the distinction between transport and kinetically limited settings that we observe. Instead, they find that soil-based weathering rates are tightly coupled to physical erosion rates across all ranges of observed denudation rate. Fig. 4 shows

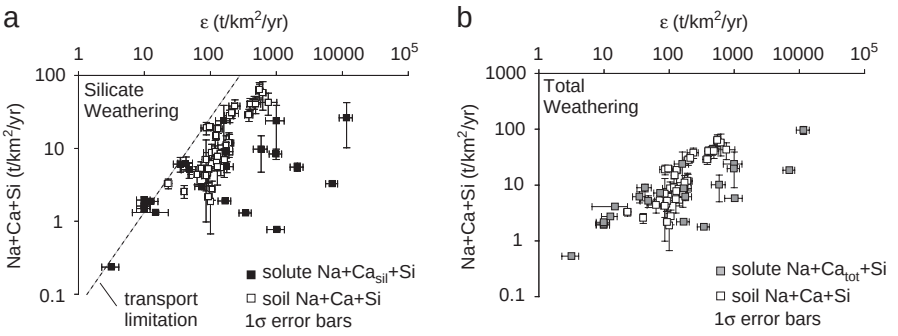

Fig. 4. Comparison of weathering rates determined by solute mass balance in surface waters (this study) with elemental depletion in soils [18]. Some differences may be expected from different study sites, but the broad trends are expected to be the same. The unexpected discrepancy may be partially but not completely attributable to Ca/Na stoichiometry of silicate weathering (the difference between a and b; see text). The remaining difference is due either to different temporal or different spatial scales, with soil depletion integrating over long time periods but not including bare rock catchments at the highest erosion rates in our compilation, where weathering is most kinetically dependent.

their data plotted along with the data from our compilation from Fig. 2. There is a clear discrepancy between the soil and solute based measurements of silicate weathering rates (Fig. 4a). In particular, they observe higher chemical weathering rates at the highest erosion rates they measure. One possible explanation is that their soil weathering rates are not adjusted for the contribution from carbonate, or that our solute-based rates are over-corrected. The Ca/Na molar ratio from soil weathering reported by Riebe et al. [18] ranges from 0.24 to 2.2, with an average of 0.90. This is much higher than the Ca/Na=0.35 assumed in calculating silicate-derived solutes (see Methods). Distinguishing between weathering of carbonate and Ca-rich silicate in the soils would require data on changes in mineral abundance.

However, even solute weathering rates uncorrected for carbonate (Fig. 4b) are significantly different from soil weathering rates, implying that weathering stoichiometry cannot alone explain the differences between the approaches. Soils measure rates integrated over much longer time scales than surface waters, which may not represent long-term average processes. Alternatively, as acknowledged by Riebe et al. [18], it is possible that soil based weathering rates do not scale to the size of entire catchments at the highest erosion rates, so that soil weathering is effectively always transport limited. Our compilation includes catchments with bare bedrock that show the greatest deviation from transport limitation; it is these catchments without any soil where the kinetic dependence of weathering is most significant and so where long-term temperature feedbacks will be most sensitive. Further work is required to understand the differences between soil and solute based estimates of weathering across a range of environments before data sets and model results can be more robustly compared.

5. Conclusions

Based on our compilation of solute-derived weathering data from catchments with diverse temperature, runoff, and denudation rates, we can quantitatively distinguish between transport and kinetically limited silicate weathering. Precise parameterization of silicate chemical weathering from such a global compilation is not expected since exact weathering mechanisms may vary in different climatic regimes, the compilation of catchments encompasses a range of rock types and the available estimates of chemical weathering and physical erosion fluxes are subject to large uncertainties. Better understanding of the functional relations of weathering mechanisms to the controlling parameters, and more and better data on silicate chemical weathering and erosion rates, are required for a more precise parameterization.

Despite the uncertainties in our parameterization, the inferred ‘activation energy’ for silicate weathering is within the range of values suggested from previous field and lab studies [7], and the dependence of silicate chemical weathering on the square root of

erosion rate and runoff to power order 1 is consistent with predicted relationships [14,31,35]. The single model that takes into account temperature, runoff, and erosion describes weathering rates in both alpine settings, with partial glacial cover and bare rock, and sub-montane catchments, with soils and vegetation. Variable soil thickness and glacial cover may in part account for deviations from the model, but these are not principal controls at the global scale, and it is not possible to determine their influence independently of the main controlling parameters. Even though glaciers produce anomalous streamwater cation chemistry [36], their impact on total rates of chemical weathering [37] can be described by the combination of accelerated physical erosion and low temperatures characteristic of glacial basins.

To first order, silicate weathering rates vary predictably depending on the total denudation rate, being controlled only by erosion rate at low erosion rates but by temperature and runoff-related kinetics at high erosion rates, as predicted in previous work [26,18,35]). This is illustrated by the upper left panel of Fig. 3. Some terrains clearly lie near the boundary between transport and weathering limited regimes, particularly when temperature and runoff are

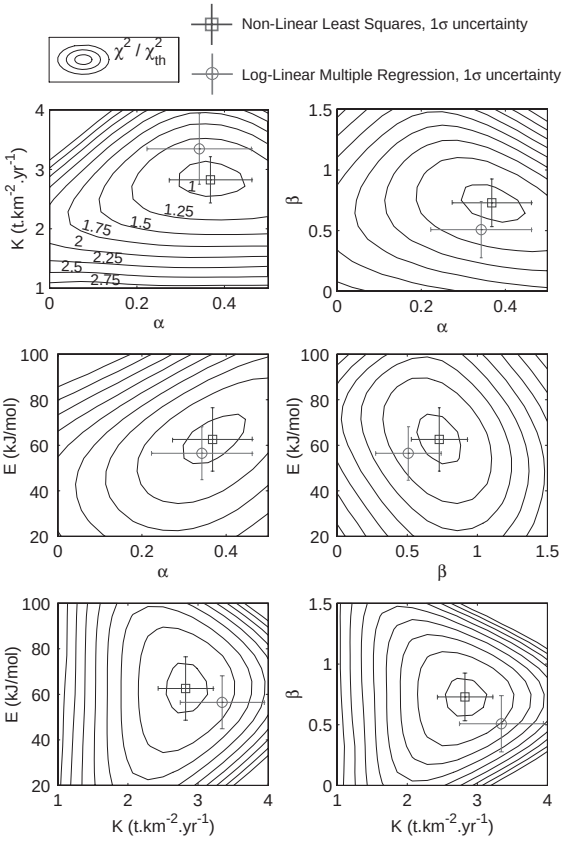

Fig. A1. Contours in parameter space of χ^2 ratioed to the theoretical value for the appropriate number of degrees of freedom (χ^2_{th}) for the function describing kinetically limited weathering (Eq. (7)), determined for four parameters (i.e. $C=0$) with 1σ errors increased by a factor of 2. Plots are similar for the function with five parameters including variable C. Contours show the minimum value of χ^2/χ^2_{th} for each combination of two parameters and thus represent projections into the 2D plane. χ^2/χ^2_{th} close to 1 for the best-fit solution suggests a good fit of the model to the data given estimated uncertainties. Best-fit solutions to our data using the log-linear multiple regression method of Riebe et al. [18] to describe soil weathering rates (open circles) are not identical but overlap the non-linear best-fit solution we have used (open squares) at the 1σ level of the parameter estimates.

low. The time scale of shifts to and from the modulation of weathering rates by soil formation in these environments remains of particular interest. The distinction of transport and weathering limited regimes reconciles previous debates about simple tectonic or climatic forcing of weathering, and offers the possibility of predicting the way that weathering relies on the production of material by erosion as well as the climatic conditions for its reaction. Application of such rate laws to predict the global response to changing climatic conditions must also take into account the additional complexities of weathering in large river basins where material is transported through a range of weathering regimes. This heterogeneity may explain the scatter that emerges in data on weathering rates at larger basin scales [19], which may integrate areas that are both kinetically and physically controlled. Calculation of the feedback between climate and silicate weathering rates must allow for the fraction of the silicate chemical weathering flux produced by landscapes in transport-limited weathering regimes. Only in the 'weathering limited regimes' will silicate weathering rates respond to changes in climate and the global response will be moderated by the fraction of the silicate chemical weathering flux derived from weathering limited regimes. Moreover, changing climatic conditions may cause shifts in the relative areas of the crust subject to these weathering limited regimes.

Acknowledgements

This work has only been possible because of the cooperation of many of the authors of cited work who made their data available. Discussions with J. Kirchner, A. White, E. Tipper, and N. Hovius, and reviews from J. Blum and R. Berner, were all helpful. This work was supported by an NSF Graduate Research Fellowship to AJW and Leverhulme Trust grants to MJB and AG.

Appendix A. Least-squares fitting

The least-squares fits to Eq. (7) with and without constant, C, were performed by standard χ^2 minimisation of the deviations in chemical weathering flux, where:

$$\chi^2 = \sum_i^N \left[\frac{\varpi_i - \varpi((\varepsilon_i, \Gamma_i, T_i), a)}{\sigma_{\varpi,i}} \right]^2 \quad (8)$$

The minimum value of χ^2 determines the optimal parameter set a, based on the observed silicate cation denudation rates (ϖ), erosion rates (ε), temperature (T), and runoff (Γ) values for each of the N total catchments. The χ^2 is weighted by an estimate of total uncertainty (σ'_ϖ) that comprises the combined uncertainties in chemical weathering (σ_ϖ) and physical erosion (σ_ε) as:

$$\sigma'_\varpi = \sqrt{\sigma_\varpi^2 + \left(\frac{\partial \varpi}{\partial \varepsilon} \sigma_\varepsilon \right)^2} \quad (9)$$

This 1σ error was increased by a factor of 2 to give a best-fit χ^2 equal to the predicted χ^2_{th} for the appropriate degrees of freedom. The quoted errors and correlation matrices (Table 4) were computed from this fit. The behaviour of χ^2 in the parameter space is shown in Fig. A1; the optimization function is well-behaved, and the best-fit solution lies at clear minimum values.

Modelling the global dataset on the basis of modern day accelerated physical denudation rates in Puerto Rico [38] makes little difference to the fits (Table A1), even though it clearly changes the interpretation of site-specific processes at this location. This emphasizes the fact that the parameterization is relatively insensitive to the uncertainties inherent in the nature of the data.

Table A1
Least-squares fits using modern day Puerto Rico denudation rates

Least-squares fit with free C, for modern day Puerto Rico denudation		Correlation coefficients				
α	0.42 ± 0.15		β	E_a	γ	**C**
β	0.75 ± 0.31	α	0.02	0.69	− 0.62	0.61
E_a	67 ± 24	β		0.25	− 0.57	0.58
K	2.40 ± 1.11	E_a			− 0.72	0.75
C	0.29 ± 0.62	γ				− 0.93

Method identical to that used in determining best fit parameters in Table 4, but using the modern day total denudation rate in Puerto Rico measured by sediment flux, rather than the estimated long-term denudation rate [38]. Differences are within the 1σ uncertainty on the fitted parameters.

References

[1] J. Ebelmen, Sur les produits de la décomposition des especes minérales de famille des silicates, Ann. Mines 7 (1845) 3–66.

[2] A.C. Lasaga, J.M. Soler, J. Ganor, T.E. Burch, K.L. Nagy, Chemical weathering rate laws and global geochemical cycles, Geochim. Cosmochim. Acta 58 (1994) 2361–2386.

[3] J.C.G. Walker, P.B. Hays, J.F. Kasting, A negative feedback mechanism for the long-term stabilisation of Earth's surface temperature, J. Geophys. Res. 86 (1981) 9776–9782.

[4] R.A. Berner, A.C. Lasaga, R.M. Garrels, The carbonate–silicate geochemical cycle and its effect on atmospheric carbon dioxide over the past 100 million years, Am. J. Sci. 283 (1983) 641–683.

[5] J. Kasting, Theoretical constraints on oxygen and carbon dioxide concentrations in the Precambrian atmosphere, Precambrian Res. 34 (1987) 205–229.

[6] G. Bluth, L. Kump, Lithologic and climatologic controls of river chemistry, Geochim. Cosmochim. Acta 58 (1994) 2341–2359.

[7] R.A. Berner, Z. Kothavala, GEOCARB III: a revised model of atmospheric CO_2 over phanerozoic time, Am. J. Sci. 301 (2001) 182–204.

[8] E.K. Berner, R.A. Berner, K.L. Moulton, Plants and mineral weathering: past and present, Treatise Geochem. 5 (2003) 169–188.

[9] H.H. Lieth, Primary production: terrestial ecosystems, Hum. Ecol. 1 (1973) 303–332.

[10] M.E. Raymo, W.F. Ruddiman, Tectonic forcing of late cenozoic climate, Nature 359 (1992) 117–122.

[11] A.F. White, A.E. Blum, Effects of climate on chemical weathering in watersheds, Geochim. Cosmochim. Acta 59 (1995) 1729–1747.

[12] Y. Huh, J.M. Edmond, The fluvial geochemistry of the rivers of Eastern Siberia: III. Tributaries of the Lena and Anabar draining the basement terrain of the Siberian Craton and the trans-Baikal Highlands, Geochim. Cosmochim. Acta 63 (1999) 967–987.

[13] C. Dessert, B. Dupré, L.M. François, J. Schott, J. Gaillardet, G. Chakrapani, S. Bajpai, Erosion of Deccan Traps determined by river geochemistry: impact on the global climate and the $^{87}Sr/^{86}Sr$ ratio of seawater, Earth Planet. Sci. Lett. 188 (2003) 459–474.

[14] P. Oliva, J. Viers, B. Dupré, Chemical weathering in granitic environments, Chem. Geol. 202 (2003) 225–256.

[15] R. Millot, J. Gaillardet, B. Dupré, C.J. Allègre, The global control of silicate weathering rates and the coupling with physical erosion: new insights from rivers of the Canadian Shield, Earth Planet. Sci. Lett. 196 (2002) 83–98.

[16] A.J. West, M.J. Bickle, R. Collins, J. Brasington, A small catchment perspective on Himalayan weathering fluxes, Geology 30 (2002) 355–358.

[17] C.S. Riebe, J.W. Kirchner, D.E. Granger, R.C. Finkel, Strong tectonic and weak climatic control of long-term chemical weathering rates, Geology 29 (2001) 511–514.

[18] C. Riebe, J.W. Kirchner, R. Finkel, Erosional and climatic effects on long-term chemical weathering rates in granitic landscapes spanning diverse climate regimes, Earth Planet. Sci. Lett. 224 (2004) 547–562.

[19] J. Gaillardet, B. Dupré, P. Louvat, C.J. Allègre, Global silicate weathering and CO_2 consumption rates deduced from the chemistry of large rivers, Chem. Geol. 159 (1999) 11018.

[20] A.J. West, Silicate Chemical Weathering: From the Himalayas to Global Models, University of Cambridge, 2005.

[21] E.T. Brown, R.F. Stallard, M.C. Larsen, G.M. Raisbeck, F. Yiou, Denudation rates determined from the accumulation of in situ-produced ^{10}Be in the Luquillo Experimental Forest, Puerto Rico, Earth Planet. Sci. Lett. 129 (1995) 193–202.

[22] J.W. Kirchner, R.C. Finkel, C.S. Riebe, D.E. Granger, J.L. Clayton, J.G. King, W.F. Megahan, Mountain erosion over 10 yr, 10 k.y., and 10 m.y. time scales, Geology 29 (2001) 591–594.

[23] A. Matmon, P.R. Bierman, J. Larsen, S. Southworth, M. Pavich, M. Caffee, Temporally and spatially uniform rates of erosion in the southern Appalachian Great Smoky Mountains, Geology 31 (2003) 155–158.

[24] M.A. Summerfield, N.J. Hulton, Natural controls of fluvial denudation rates major world drainage basins, J. Geophys. Res. 99B (1994) 13871–13883.

[25] M.A. Carson, M.J. Kirkby, Hillslope Form and Process, Cambridge University Press, Cambridge, UK, 1972, 475 pp.

[26] R.F. Stallard, J.M. Edmond, Geochemistry of the Amazon: 2. The influence of geology and weathering environment on the dissolved-load, J. Geophys. Res. 88 (1983) 9671–9688.

[27] S.R. Taylor, S.M. McLennan, The Continental Crust: Its Composition and Evolution, Blackwell, Oxford, UK, 1985, 312 pp.

[28] A.F. White, Chemical weathering rates of silicate minerals in soils, in: A.F. White, S.L. Brantley (Eds.), Reviews in Mineralogy, vol. 31, Mineralogical Society of America, Chelsea, 1995, pp. 407–461.

[29] A.D. Jacobson, J.D. Blum, Relationship between mechanical erosion and CO_2 consumption in the New Zealand Southern Alps, Geology 31 (2003) 865–868.

[30] A. Taylor, J.D. Blum, Relation between soil age and silicate weathering rates determined from the chemical evolution of a glacial chronosequence, Geology 23 (1995) 979–982.

[31] A.F. White, S.L. Brantley, The effect of time of the weathering of silicate minerals: why do weathering rates differ in the laboratory and field? Chem. Geol. 202 (2003) 479–506.

[32] P. Brady, S. Carroll, Direct effects of CO_2 and temperature on silicate weathering—possible implications for climate control, Geochim. Cosmochim. Acta 58 (1994) 1853–1856.

[33] C. Riebe, J.W. Kirchner, R. Finkel, Sharp decrease in long-term chemical weathering rates along an altitudinal transect, Earth Planet. Sci. Lett. 218 (2004) 421–434.

[34] C.S. Riebe, J.W. Kirchner, R.C. Finkel, Long-term rates of chemical weathering and physical erosion from cosmogenic nuclides and geochemical mass balance, Geochim. Cosmochim. Acta 67 (2003) 4411–4427.

[35] L.R. Kump, S.L. Brantley, M.A. Arthur, Chemical weathering, atmospheric CO_2, and climate, Annu. Rev. Earth Planet. Sci. 28 (2000) 611–667.
[36] S.P. Anderson, J.I. Drever, C.D. Frost, P. Holden, Chemical weathering in the foreland of a retreating glacier, Geochim. Cosmochim. Acta 64 (2000) 1173–1189.
[37] S.P. Anderson, Glaciers show direct linkage between erosion rate and chemical weathering fluxes, Geomorphology 67 (2005) 147–157.
[38] B.F. Turner, R.F. Stallard, S.L. Brantley, Investigation of in situ weathering of quartz diorite bedrock in the Rio Icacos basin, Luquillo Experimental Forest, Puerto Rico, Chem. Geol. 202 (2003) 313–341.
[39] D. York, Least squares fitting of a straight line with correlated errors, Earth Planet. Sci. Lett. 5 (1969) 320–324.
[40] C. Picouet, B. Dupre, D. Orange, M. Valladon, Major and trace element geochemistry in the upper Niger river (Mali): physical and chemical weathering rates and CO_2 consumption, Chem. Geol. 185 (2002) 92–124.
[41] J.M. Edmond, M.R. Palmer, C.I. Measures, B. Grant, R.F. Stallard, The fluvial geochemistry and denudation rate of the Guayana Shield in Venezuela, Colombia, and Brazil, Geochim. Cosmochim. Acta 59 (1995) 3301–3325.
[42] J.L. Clayton, W.F. Megahan, Erosional and chemical denudation rates in the southwestern Idaho Batholith, Earth Surf. Processes Landf. 11 (1986) 389–400.
[43] A. Hodson, M. Tranter, G. Vatne, Contemporary rates of chemical denudation and atmospheric CO_2 sequestration in glacier basins: an Arctic perspective, Earth Surf. Processes Landf. 25 (2000) 1447–1471.
[44] R. Hosein, K. Arn, P. Steinmann, T. Adatte, K.B. Fllmi, Carbonate and silicate weathering in two presently glaciated, crystalline catchments in the Swiss Alps, Geochim. Cosmochim. Acta 68 (2004) 1021–1033.
[45] A.J. Hodson, P. Porter, A. Lowe, P.N. Mumford, Chemical denudation and silicate weathering in Himalayan glacier basins: Batura Glacier, Pakistan, J. Hydrol. 262 (2002) 193–208.
[46] A. Galy, C. France-Lanord, Higher erosion rates in the Himalaya: geochemical constraints on riverine fluxes, Geology 29 (2001) 23–26.
[47] J. Gaillardet, B. Dupré, C.J. Allègre, A global geochemical mass budget applied to the Congo Basin rivers: erosion rates and continental crust composition, Geochim. Cosmochim. Acta 59 (1995) 3469–3485.
[48] J. Viers, B. Dupre, J. Braun, S. Debert, B. Angeletti, J.N. Ngoupayou, A. Michard, Major and trace element abundances, and strontium isotopes in the Nyong basin river (Cameroon), Chem. Geol. 169 (2000) 211–241.
[49] L.J. Zeman, O. Slaymaker, Mass balance model for calculation of ionic input loads in atmospheric fallout and discharge from a mountainous basin, Hydrol. Sci. Bull. 23 (1978) 103–117.
[50] H. Grip, A. Malmer, F.K. Wong, Converting tropical rain forest to forest plantation in Sabah Malaysia: Part I. Dynamics and net losses of nutrients in control catchment streams, Hydrol. Process. 8 (1994) 179–194.
[51] J.J. Stoorvogel, Gross Inputs and Outputs of Nutrients in Undisturbed Forest, Tai Area, Cote d'Ivoire, Tropenbos Foundation, Wageningen, Netherlands, 1993.
[52] D. Vance, M.J. Bickle, S. Ivy-Ochs, P. Kubik, Erosion and exhumation in the Himalaya from cosmogenic isotope inventories of river sediments, Earth Planet. Sci. Lett. 206 (2003) 273–288.
[53] J.K. Sueker, D.W. Clow, J.N. Ryan, R.D. Jarrett, Effect of basin physical characteristics on solute fluxes in nine alpine/subalpine basins, Colorado, USA, Hydrol. Process. 15 (2001) 2759–2769.
[54] D.P. Dethier, W. Ouimet, P. Bierman, R. Finkel, Long-term erosion rates derived from ^{10}Be in sediment from small catchments, North Front Range and Southern Wyoming, GSA Fall Meeting, 2002.
[55] B. Hallet, L. Hunter, J. Bogen, Rates of erosion and sediment evacuation by glaciers: a review of field data and their implications, Glob. Planet. Change 12 (1996) 213–235.